Fuzzy Spectral and Spatial Feature Integration for Classification of Nonferrous Materials in Hyperspectral Data

Artzai Picón, Ovidiu Ghita, Paul F. Whelan, *Senior Member, IEEE*, and Pedro M. Iriondo

***Abstract*—Hyperspectral data allows the construction of more elaborate models to sample the properties of the nonferrous materials than the standard RGB color representation. In this paper, the nonferrous waste materials are studied as they cannot be sorted by classical procedures due to their color, weight and shape similarities. The experimental results presented in this paper reveal that factors such as the various levels of oxidization of the waste materials and the slight differences in their chemical composition preclude the use of the spectral features in a simplistic manner for robust material classification. To address these problems, the proposed FUSSER (FUzzy Spectral and Spatial classifiER) algorithm detailed in this paper merges the spectral and spatial features to obtain a combined feature vector that is able to better sample the properties of the nonferrous materials than the single pixel spectral features when applied to the construction of multivariate Gaussian distributions. This approach allows the implementation of statistical region merging techniques in order to increase the performance of the classification process. To achieve an efficient implementation, the dimensionality of the hyperspectral data is reduced by constructing bio-inspired spectral fuzzy sets that minimize the amount of redundant information contained in adjacent hyperspectral bands. The experimental results indicate that the proposed algorithm increased the overall classification rate from 44% using RGB data up to 98% when the spectral-spatial features are used for nonferrous material classification.**

***Index Terms*—Hyperspectral image processing, image classification, spectral fuzzy sets.**

I. Introduction

NOWADAYS, sustainable development has become one of the most important paradigms of the contemporary societies since a large amount of electrical and electronic equipment is being designed, manufactured and retired. Thus, the problem of processing and recycling the electrical and electronic waste is of paramount importance since this type of waste is not biodegradable and may be contaminated with highly toxic substances.

Currently, the recycling process is carried out in generic dumps where the electronic waste is mixed among other waste materials. While a wide variety of materials are used to manufacture the electrical and electronic products, the process required to recycle the waste from electrical and electronic equipment (WEEE) is one of the most complex and labor intensive industrial tasks.

In recent years, due to the environmental legislation that has been introduced in regard to the recycling process for WEEE, the development of systems that are able to sort and process the electrical and electronic waste in an automatic fashion has been viewed as the most cost-effective recycling solution. For instance, the EC WEEE Recycling Directive [1] states that all EU countries have to recover about 70%–80% of the weight of the produced WEEE and to reuse 50%–75% of the recovered materials or components. This law strengthened the necessity to devote additional efforts in the development of new techniques and technologies that are able to improve the performance of the methods that are currently applied for WEEE recycling.

After the WEEE scrap is subjected to shredding, magnetic, mechanical and densiometric sorting, the resulting waste fractions still contain a mix of nonferrous metals (e.g., aluminum, copper, zinc, brass, and lead) and austenitic Stainless Steel (Fig. 1) representing approximately 13% of the total WEEE weight. It is important to mention that the nonferrous and austenitic Stainless Steel cannot be identified and separated using the current recycling methods [2], [3].

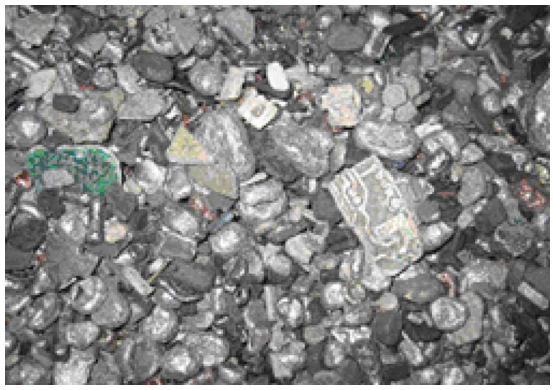

Fig. 1. Fractions of different nonferrous metals and Stainless Steel resulting from the WEEE recycling process.

Manuscript received April 27, 2009; revised June 22, 2009; accepted August 19, 2009. First published September 15, 2009; current version published November 06, 2009. This work was supported in part by the Etortek Program of the Basque Government. Part of this work was carried out while A. Picón was a Visiting Researcher at the Centre for Image Processing and Analysis (CIPA), Dublin City University, from February 2007 to February 2008. Paper no. TII-09-04-0057.R1.

A. Picón is with the Infotech Unit, Tecnalia Research Corporation, Zamudio, Bizkaia 48170, Spain (e-mail: apicon@robotiker.es).

O. Ghita and P. F. Whelan are with the Centre for Image Processing and Analysis, School of Electronic Engineering, Dublin City University, Ireland (e-mail: ghitao@eeng.dcu.ie; paul.whelan@dcu.ie).

P. M. Iriondo is with the Department of Automatic Control and Systems Engineering, ETSI of Bilbao, University of the Basque Country UPV-EHU, Spain (e-mail: pedro.iriondo@ehu.es).

Color versions of one or more of the figures in this paper are available online at http://ieeexplore.ieee.org.

Digital Object Identifier 10.1109/TII.2009.2031238

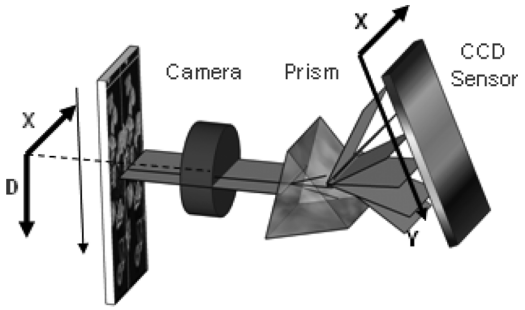

Fig. 2. The hyperspectral image acquisition process.

As the price of the recycled materials largely depends on purity, the nonferrous fractions resulting after WEEE recycling are currently sold at a much lower price and their reutilization is more difficult. A proper separation of these nonferrous metals will allow a substantial increase in the added value of the whole recycling process and helping the EU countries to comply with the 2002/96/EC directive.

The methods that are currently applied to separate the nonferrous metals and Stainless Steel involve a visual inspection based on the color properties associated with the analyzed materials [4]. In this regard, Kutila *et al.* [5] developed a color inspection system that was applied to separate the metals whose colors are predominantly red (brass, copper) from the bright metals such as Stainless Steel, aluminum and zinc. The experiments reported in their paper indicate that the materials defined by red properties can be separated from the materials with bright colors (reported classification accuracy 83.5%), but the results were inaccurate when they attempted to separate the metals with similar chromatic properties (the reported classification accuracies for materials such as copper and brass dropped to 37.4% and 36.8%, respectively). X-Ray methods have been widely used for metal scrap and plastic sorting [6], [7]. However, the application of X-Ray backscatter imaging to tasks such as the sorting of nonferrous materials in industrial environments may encounter difficulties as this technology only measures the material density [4]. The only methods that proved efficient in classifying nonferrous metals are based on the analysis of the spectrum emitted by metals after they were subjected to thermal stress [8]. These methods cannot be used for recycling purposes due to the low speed of the spectrum acquisition process and the technical difficulties to devise a suitable excitation method for each WEEE nonferrous fraction.

Modern optical spectrometers overcome these problems as they provide high-resolution spatial image data with a detailed spectral accuracy (see Fig. 2). This technology involves the capture and interpretation of multidimensional digital images and the current range of spectral imaging systems is able to capture multiple bands from ultraviolet to far infrared with good bandwidth resolution. This versatility enables the application of the spectral imaging systems in the detection and classification of various natural and man-made materials such as minerals, metals, plastic, vegetation, etc., [7], [9]–[11]. Recently, spectral data has been used to model the characteristics of the human tissues when applied to the development of robust face discriminators [12] and to properly characterize welding defects using a hybrid neural network-fuzzy-logic approach [13].

A characteristic of the hyperspectral images is that each pixel is defined by a vector whose elements are the different spectral (wavelengths) components captured from the scene. This hyperspectral vector provides not only the color information associated with the scene, but also information in regard to the chemical composition of the scene materials [9], [14]–[16].

To distinguish among different spectrums, several similarity measures were proposed in the literature on hyperspectral data analysis [17]. The classical approaches that evaluate the distances between various spectrums in the $\mathbf{R}^n$ Euclidean space or those based on the measurement of the angle between spectrums' Spectral Angle Mapper (SAM) [18] offer a good estimation in regard to the similarity of two spectrums, but they do not analyze the correlation between the data contained in adjacent spectral bands [9]. Consequently, these approaches are not able to properly accommodate the intraclass variations that are generated by the spectral differences between samples that belong to the same material. (In the context of material classification the intraclass variations are caused by external factors including metal oxidization, nonuniform illumination conditions, specular highlights, shadows, etc.)

The intraclass variations can be appropriately modeled by the use of pattern recognition techniques since the spectral information is evaluated in a more elaborate fashion [15], [19]. One problem that has to be addressed is the high dimensionality of the hyperspectral data [20]–[22]. In this sense, to circumvent the problems caused by the large resolution of the hyperspectral data when used for classification purposes, feature reduction techniques are usually applied to avoid the Hughes phenomenon [23]. To this end, the information contained in the spectral bands can be either decorrelated using principal component analysis (PCA) [20], wavelet decomposition [24]–[26], or by applying user-defined band selection [22], [27], [28]. Once the hyperspectral data is decorrelated, the feature vectors describing the spectrum are extracted and used for classification tasks. Typically, the feature vectors are constructed using the spectral information associated with each pixel in the image [29]–[31], but recent approaches suggested to merge the spectral and spatial information in order to increase the classification accuracy [32]–[34].

In this paper, we propose to use hyperspectral data to separate different nonferrous materials using feature vectors that sample the material characteristics in the spectral-spatial domain. This paper is organized as follows. In Section II, an overview of the developed material classification system is detailed where the key issue is the application of the spectral fuzzy sets for hyperspectral data decorrelation. This approach uses the physical properties of the spectrums to overcome some of the limitations associated with other decorrelation methods such as PCA and linear discriminant analysis (LDA) among others. Building on this concept, spectral-spatial features are constructed to model the characteristics of the nonferrous materials by the use of spatial fuzzy histograms. Sections III and IV detail the classification process and introduce the statistical region merging approach that is applied to join the connected regions with similar properties. Section V details the experimental results, while in Section VI concluding remarks are provided.

II. System Overview

This section outlines the complete procedure that has been developed to extract the feature vectors from the acquired spectral images. Also, in this section, we explain how the spectral-spatial features are used for nonferrous material classification.

The proposed algorithm, called FUzzy Spectral and Spatial feature classifiER (FUSSER), can be divided into two main components. The first component, as illustrated in Fig. 3, performs the normalization and decorrelation of the spectrum and the spectral-spatial feature merging. The computational stages associated with the first component of the algorithm can be summarized as follows.

1) Image acquisition.
2) Data normalization.
3) Spectral decorrelation.
4) Spectral-spatial feature integration.
5) First-stage classification.

As illustrated in Fig. 3, the captured spectral image data is subjected to intensity normalization, filtering and decorrelation. Different decorrelation techniques such as PCA, LDA, Wavelet decomposition and the proposed spectral fuzzy sets are analyzed in our study. This is followed by the calculation of the spectral-spatial features by constructing fuzzy histograms in predefined neighborhoods for each pixel in the decorrelated image data. Finally, the extracted feature vectors are fed into the first-stage classifier which creates an initial partition of the image with respect to the materials contained in the image data.

The second component of the developed algorithm, as illustrated in Fig. 4, implements a statistical reclassification and region merging approach that is applied to refine the initial partition of the image resulting from the first component (see Fig. 3) of the material classification algorithm.

A. Image Acquisition and Light Normalization

The acquired spectral data is represented by an image matrix where each element (pixel) at position (x, y) is represented by a vector $\mathbf{L}$. Let $\mathbf{L}$ be the vector representation of the spectrum defined by the intensity responses of the K wavelengths and $\mathbf{W}$ and $\mathbf{B}$ be the vectors representing the white and black references of the spectrum, as illustrated in Fig. 5

$$\mathbf{L} = \{L_1, L_2, \ldots, L_K\}^T \tag{1}$$
$$\mathbf{W} = \{W_1, W_2, \ldots, W_K\}^T \tag{2}$$
$$\mathbf{B} = \{B_1, B_2, \ldots, B_K\}^T. \tag{3}$$

In order to make the spectral vector $\mathbf{L}$ independent to the illumination source, a solution is to normalize the hyperspectral data using a dichromatic model such as that proposed by Shafer [35]. Shafer's illumination model assumes that the white illumination reference is known, but this approach is difficult to be directly applied to the normalization of the hyperspectral data due to the complications associated with the development of a light source that has the same emittance for each wavelength. To be able to implement the Shafer's model when dealing with nonwhite hyperspectral illumination, in our implementation, we have adopted the approach proposed by Tan *et al.* [36]. In this approach, the spectral components of the incident light are calculated at each location as illustrated in (4) and the spectrum is normalized using (5)

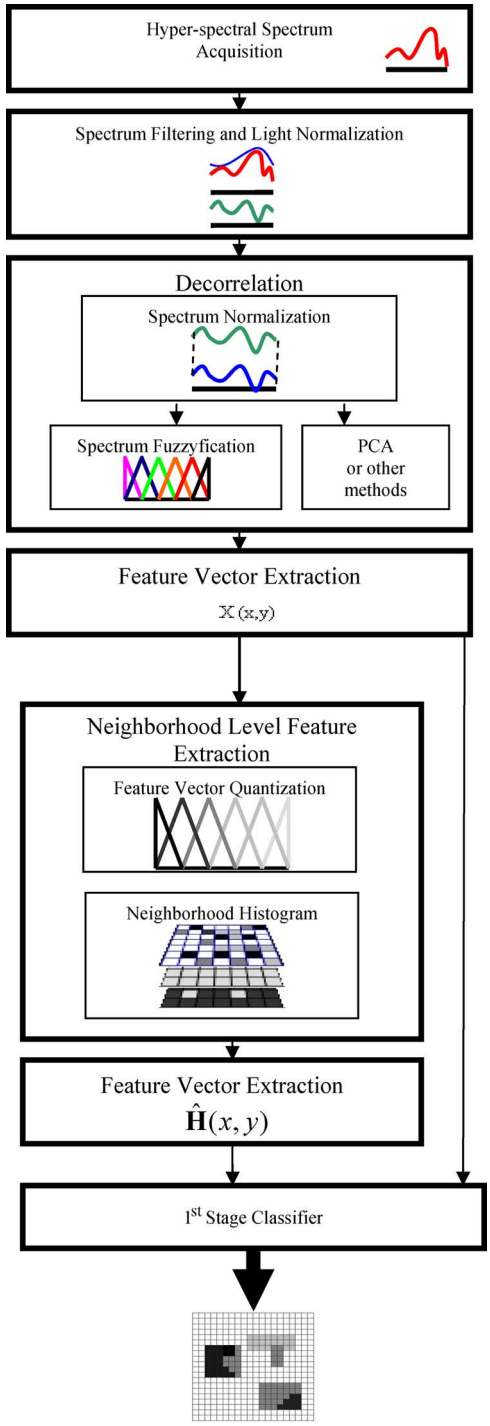

Fig. 3. Outline of the first component of the FUSSER algorithm.

$$C_{light}(\lambda_i) = \frac{L_{light}(\lambda_i)}{\sum_{j=1}^{k} L_{light}(\lambda_j)} \tag{4}$$
$$\hat{L}(\lambda_i) = \frac{L(\lambda_i)}{C_{light}(\lambda_i)}. \tag{5}$$

Since $L_{\text{light}}(\lambda)$ is not known for each pixel in the hyperspectral data, the spectrum normalization will be indirectly performed

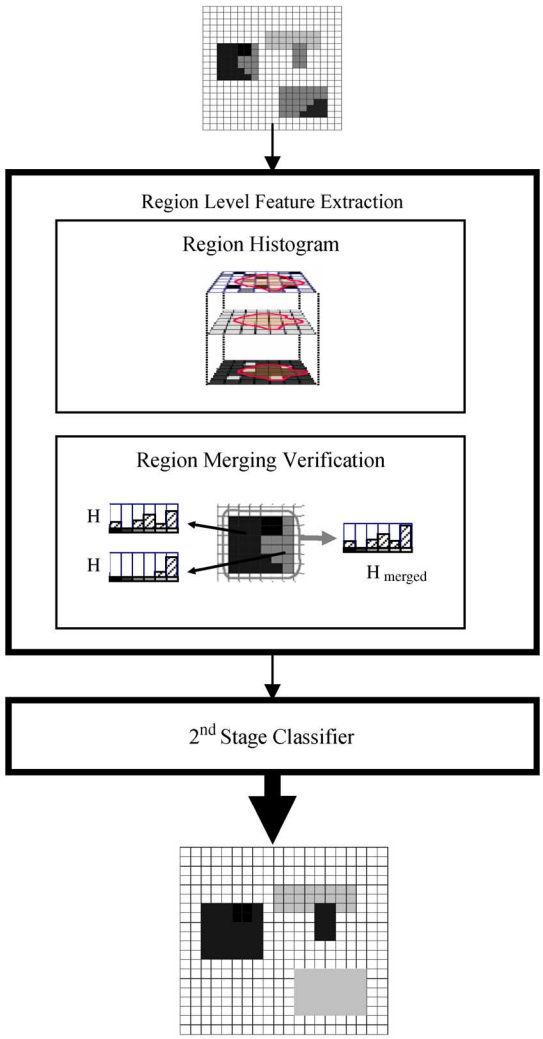

Fig. 4. Outline of the second component of the FUSSER algorithm.

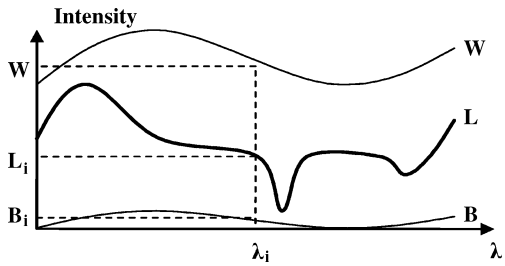

Fig. 5. Hyperspectral vector (L), white reference (W), and black reference (B) of the spectrum.

using the reflections of the white $(\mathbf{W})$ and black reference $(\mathbf{B})$ as follows:

$$\hat{L}(\lambda_i) = \frac{L(\lambda_i) - B}{W - B}. \tag{6}$$

Geusebroek *et al.* [29] demonstrated that the highlights and shadows caused by the object geometry, material reflectance, and position of the light source can be compensated for by applying intensity normalization and desaturation. Using this concept, in our implementation each spectrum is first normalized by its mean and afterwards it is desaturated by the subtraction of its minimum value (7), as a variation of the method proposed by Stockman to extract the Spectral hue [37]

$$L_{\text{norm}}(\lambda_j) = L_N(\lambda_j) - \min_{i\in[1,k]}(L_N(\lambda_i)) \tag{7}$$

where $L_N(\lambda_j) = \hat{L}(\lambda_j)/\sum_{m=1}^{k}\hat{L}(\lambda_m)$ and $j \in [1,k]$.

B. Spectral Decorrelation

Since the hyperspectral data is high dimensional and is characterized by a high level of redundancy, there is a significant overlap between the spectral distributions associated with different nonferrous materials. In order to reduce the level of redundancy in the hyperspectral data and improve the material separation, decorrelation techniques are applied to obtain a new data representation that has a reduced dimensionality. In this study different decorrelation methods are investigated, namely the PCA-based approach [20], [26], LDA [19], [43], automatic band selection [47], wavelet decomposition [25], and a novel technique based on spectral fuzzyfication that will be detailed in this paper.

PCA allows the extraction of highly discriminative features by performing an orthogonal decomposition of the hyperspectral data. The main disadvantage associated with the PCA and related techniques such as LDA and independent component analysis (ICA) [44] is that they require a training procedure that involves sampling relevant data-points from the high-dimensional data. Another disadvantage of PCA resides in the fact that the compressed feature vectors are not directly linked with concrete physical variables and as a result they cannot be easily interpreted. Also, PCA requires retraining if new materials are included in the classification process.

To overcome the limitations associated with classical decorrelation techniques, a new method based on spectral fuzzyfication has been designed to optimize the discriminative power of the spectral features using an approach suggested by the human visual system when applied to the classification of nonferrous materials.

1) Classical Decorrelation Methodologies: The first decorrelation method analyzed in this paper is based on the widely used PCA (also referred in the computer vision literature to as Karhunen–Loève transform) technique [20], [38], [39]. PCA is a vector transform whose aim is to reduce the dimensionality of the input data by projecting it onto a lower dimensional orthogonal representation.

An adequate number of normalized vectors covering each class associated with nonferrous materials are selected from training data in order to calculate the eigenvectors and eigenvalues of their covariance matrix [39]. The first $M < K$ eigenvectors $\{\hat{\mathbf{u}}_1, \hat{\mathbf{u}}_2, \hat{\mathbf{u}}_3, \ldots \hat{\mathbf{u}}_M\}$ calculated from the covariance matrix are used to generate the transformation matrix $\mathbf{V}$. The PCA vector transform involves the projection of the high-dimensional vectors on the transformation matrix $\mathbf{V}$, as shown in (8)

$$\begin{aligned}\mathbf{X} &= \mathbf{V}^t(\mathbf{L}_{\text{norm}} - \overline{\mathbf{L}}_{\text{norm}}) \\ &= [\hat{\mathbf{u}}_1, \hat{\mathbf{u}}_2, \hat{\mathbf{u}}_3, \ldots \hat{\mathbf{u}}_M]^{\mathrm{T}} \cdot (\mathbf{L}_{\text{norm}} - \overline{\mathbf{L}}_{\text{norm}})\end{aligned} \tag{8}$$

where $\mathbf{L}_{\text{norm}}$ is the normalized vector to be transformed, $\overline{\mathbf{L}}_{\text{norm}}$ is the mean vector of all normalized vectors selected for training

and $\mathbf{V}$ is the eigenmatrix defined by the first M eigenvectors calculated from the covariance matrix of the training vectors.

After the application of the PCA transformation, the spectrum is represented by $\mathbf{X}$ vectors in the orthogonal PCA space. This representation offers a decorrelated and compressed version of the original hyperspectral data that can be efficiently used for classification tasks. For comparative purposes, in this paper, we also included the LDA, Wavelet and automatic band selection techniques to assess their performance when applied for data decorrelation.

2) Spectral Fuzzy Sets: The method proposed in this paper to decorrelate the hyperspectral data is based on the knowledge that the adjacent wavelengths of the spectrum are more correlated than the distant wavelengths. This observation is justified since for most solid materials the spectral information varies smoothly over successive spectral wavelengths [46]. Consequently, the spectral characteristics associated with nonferrous materials are sampled by groups of adjacent spectral bands rather than unique spectral bands. To model this property, the intensity values for each wavelength have to take into account the values of the adjacent wavelengths. This can be obtained by dividing the spectrum in separate groups to attain the desired spectral selectivity. To avoid the problems caused by a crisp division of the spectrum, in this paper a method based on the spectrum fuzzyfication is proposed. This involves the separation of the hyperspectral data into a number of fuzzy groups where each group covers a range of wavelengths and the contribution of each wavelength is modeled by a membership function.

Let $\mathbf{L}_{\text{norm}}$ be the K normalized components of the spectrum as defined in (7) and M be the number of fuzzy sets in which the spectrum will be divided. A membership function is defined for each of the fuzzy sets to characterize the membership for any wavelength in the spectrum to its related fuzzy set. For the sake of simplicity, in this implementation, triangular shaped membership functions are used (for a systematic approach in regard to the construction of the fuzzy rules the reader is directed to [41], [42]). In this way, the membership value for each point of the spectrum is defined by a triangular function that is defined as follows:

$$Mf_i(\lambda) = \begin{cases} 1 - \left|\frac{\lambda - \lambda_{Ci}}{D}\right|, & \lambda_{Ci} - D < \lambda < \lambda_{Ci} + D \\ 0, & \text{otherwise} \end{cases} \quad (9)$$

where λ_{Ci} is the central wavelength value of the fuzzy set i and D defines the separation between two consecutive central wavelengths, as shown in Fig. 6.

As illustrated in Fig. 6, each of the spectrum wavelengths has a membership grade to each of the segregated fuzzy sets. In other words, each wavelength has a membership grade different than zero in the two adjacent groups and a membership grade of zero in the rest of the groups. This is shown in Fig. 7.

The data resulting after the application of the fuzzy set representation to the initial hyperspectral data is defined by the *Energy* of each fuzzy set that is calculated by weighting the intensity of each of the spectrum elements $(L_{\text{norm}}(\lambda_i))$ with the membership function associated with each fuzzy set as follows:

$$E_i = \int_{\lambda=0}^{\lambda=K} Mf_i(\lambda) \cdot L_{\text{norm}}(\lambda) d\lambda \quad (10)$$

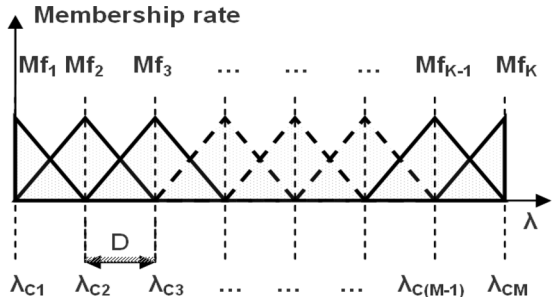

Fig. 6. Triangle shaped membership functions.

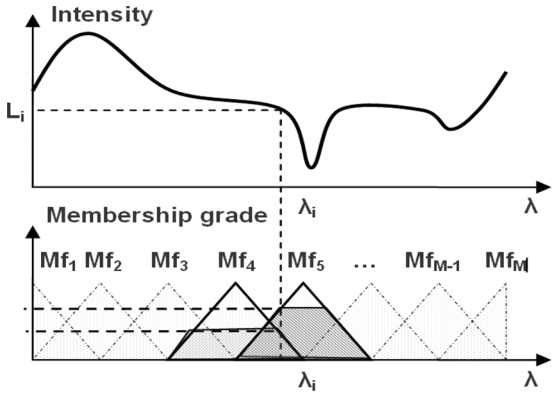

Fig. 7. An example that illustrates the membership grade associated with the wavelength λ_i.

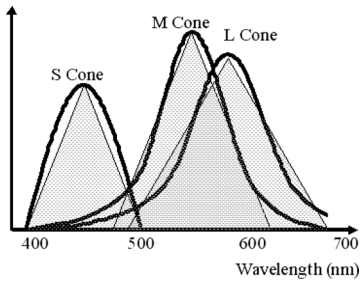

Fig. 8. Sensitivity of the human retinal receptors.

The *Energy* measure defined in (10) samples the intensity of the spectrum in each of the fuzzy sets. Based on the value of *Energy* for each fuzzy set, we can obtain useful information in regard to the radiometric (spectral) properties of the nonferrous materials contained in the hyperspectral image data. In this way, each hyperspectral pixel is defined by a vector containing the *Energy* values of the M fuzzy sets, as illustrated in (11)

$$\mathbf{X} = \{E_1, E_2, \ldots, E_M\}^T \quad (11)$$

This fuzzy representation allows us to characterize the spectral information in an efficient manner since the spectral features are not affected by the appropriate selection of the training elements as it is the case with the classical data decorrelation techniques. In addition, the dimensionality of the hyperspectral data is optimally reduced since the fuzzyfication procedure maximizes the decorrelation between adjacent spectral bands, but at the same time maintains the physical meaning of the spectral features.

This approach is closely related to the way the human eye extracts the color information where each *Energy* value can be

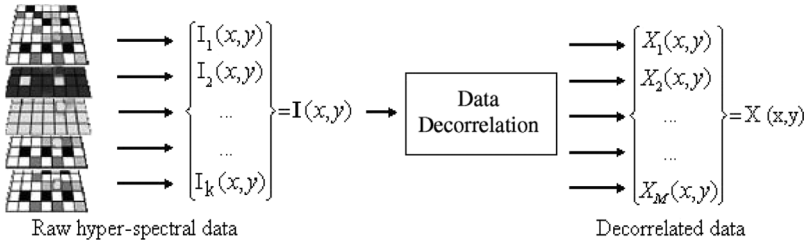

Fig. 9. Vectorial representation of the hyperspectral image data.

conceptualized as the amount of data absorbed by a color receptor (cone) present in the human visual system. The chromatic retinal receptors consist of three different types of cones, where each cell (cone) is able to convert the electromagnetic radiation emitted by the surface of the objects into chromatic information [46]. Each of these cones, as shown in Fig. 8, responds strongly to different parts of the spectrum ($S = \text{blue}$, $M = \text{green}$, $L = \text{red}$) and the colors sensed by humans are created as a combination of the three primary colors (R,G,B) given by the response of each type of cone. It is interesting to note that the chromatic receptors present in the human eye employ models that are consistent with the fuzzy set theory. Our approach based on the construction of spectral fuzzy sets can be viewed as an extension of the process applied by the human vision system to attain the trichromatic information to the hyperspectral case.

The decorrelated feature vectors defined in (11) contain only spectral information and they do not provide any spatial information (see Fig. 9).

Since the spatial information provides additional cues in characterizing the properties associated with nonferrous materials, the development of a feature vector that encompasses the spatial and spectral information can increase the discrimination between different nonferrous materials. To achieve this goal, fuzzy spatial histograms are proposed to merge the spectral and spatial features into a compound feature vector. These histograms encompass the distribution of the spectral vectors $\mathbf{X}$ [see (8) and (11)] in a given neighborhood or region.

C. Vector Quantization

Although the components X_i of the spectral vectors $\mathbf{X}$ obtained after the application of the decorrelation techniques (based either on PCA or spectrum fuzzyfication) can be theoretically used to model the spectral properties of the nonferrous materials, in practice they need to be quantized prior to the calculation of the feature histograms that integrate the spectral and spatial information. This approach is motivated by the fact that due to noise, various illumination conditions, and various levels of oxidization, the spectral pixels that are sampled from same material very seldom have identical intensities values and these uncertainties between same-material pixels may cause severe classification errors.

The classical approach to calculate the spectral-spatial features involves the binning of the X_i values in a feature histogram that is calculated over a predefined neighborhood in the image. This approach returns inappropriate results since the spectral components X_i show little variation among nonferrous materials and the simplistic crisp binning process can induce erratic changes in the histograms if the intensity values of the X_i components are in the vicinity of the borders between bins. To address this issue, we generate a normalized representation, where each component X_i of the spectral vectors $\mathbf{X}$ is mapped into a vector by the use of fuzzy membership functions. Using this approach, each spectral component X_i generates a quantized vector where the elements of the vector represent the grade of membership of the intensity value X_i with respect to the M fuzzy sets that are applied to sample the hyperspectral domain. The proposed fuzzy-based quantization procedure is illustrated in Fig. 10. This fuzzy-based representation has the advantage that the variations between the spectral components X_i and the uncertainties caused by noise or different levels of material oxidization are better modeled than in the case when crisp binning would be employed.

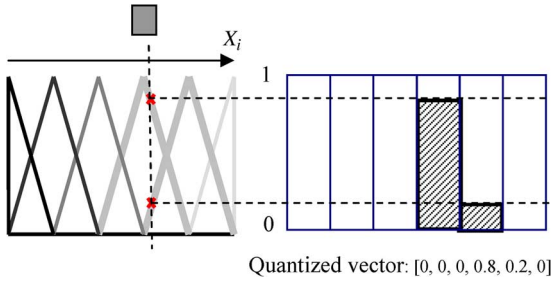

Fig. 10. The fuzzy-based vector quantization procedure. This diagram illustrates the calculation of the quantized vectors when six fuzzy sets are employed to sample the hyperspectral domain.

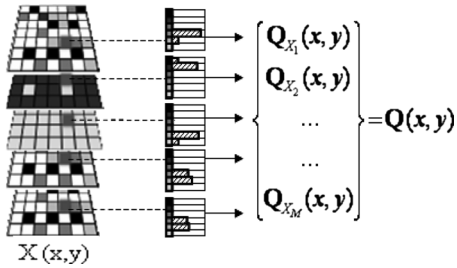

Fig. 11. Quantization of a spectral pixel.

The quantization procedure shown in Fig. 10 is performed for each component of the spectral pixel and the quantization vector $\mathbf{Q}(x, y)$ is created by concatenating the quantization vectors resulting from each component X_i of the spectral vector $\mathbf{X}$, as illustrated in Fig. 11.

D. Spectral-Spatial Features Integration

To construct the spectral-spatial histogram we need to define a neighborhood around each spectral pixel. In this way, a fuzzy histogram is computed using the quantized vectors $\mathbf{Q}$ that are calculated, as illustrated in Fig. 11, for all spectral pixels contained in the neighborhood

$$\mathbf{H}(x,y) = \sum_{i=x-A/2}^{x+A/2} \sum_{j=y-B/2}^{y+B/2} \mathbf{Q}(i,j). \tag{12}$$

The histogram $H(x,y)$ shown in (12) encodes the spatial distribution for each spectral component X_i inside the selected neighborhood (size $\mathrm{A} \times \mathrm{B}$) and the spectral characteristics associated with nonferrous materials are captured by the histogram's shape.

It is useful to note that (12) generates the same result as in the case when the fuzzy histogram is calculated for each channel X_i independently and the resulting spectral histograms are concatenated into a single vector. However, the implementation described in (12) has the advantage that allows the calculation of the histograms for different sized neighborhoods by just performing additive operations. This property is very useful for our implementation since the compound descriptor characterizing two regions would be the same as the sum of the descriptors that are calculated for each region individually. This opens the possibility of real-time implementation for the region merging procedure that will be detailed in Section IV.

III. Classification Procedure

In the previous section, the procedure that is applied to obtain the feature vectors that encompass the spectral and spatial features has been detailed. The histogram vector shown in (12) defines the distribution of the spectral information in a predefined neighborhood around the pixel (x,y) and is used as input for classification. In our implementation, the multivariate Gaussian classifier is proposed to perform the material classification since the Gaussian distributions approximate well the dispersion of the spectral-spatial feature vectors within each class of nonferrous materials.

A Gaussian model for each material is created where $\boldsymbol{\mu}$ and $\boldsymbol{\Sigma}$ are the mean vector and the covariance matrix of the modeled class

$$N\left(\mathbf{x}|\boldsymbol{\mu}, \sum\right) = \frac{1}{(2\cdot\pi)^{D/2}} \frac{1}{|\sum|^{1/2}} e^{\left\{-\frac{1}{2}(\mathbf{x}-\boldsymbol{\mu})^T \sum^{-1}(\mathbf{x}-\boldsymbol{\mu})\right\}}. \tag{13}$$

The classification stage is carried out by checking each spectral-spatial vector $H(x,y)$ calculated for each pixel in the image against the normalized distributions that define each material class. Each pixel in the decorrelated hyperspectral image is labeled to the class that achieves the minimum matching cost.

IV. Region Merging

The aim of the first-stage classification is to label each pixel in the image with respect to the nonferrous material classes. Our investigations revealed that due to interclass overlap some pixels are misclassified. The errors in classification were mostly caused by strong highlights and various oxidization levels encountered for similar materials.

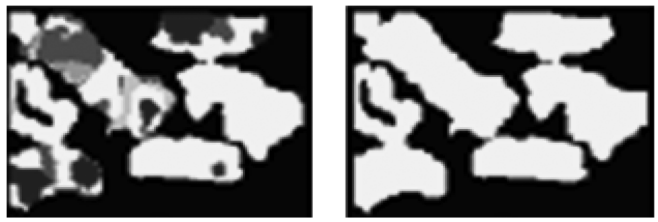

(a) (b)

Fig. 12. (a) Classification results obtained when the neighborhood fuzzy histograms are used as input vectors. (b) Classification results obtained after the application of the region merging procedure.

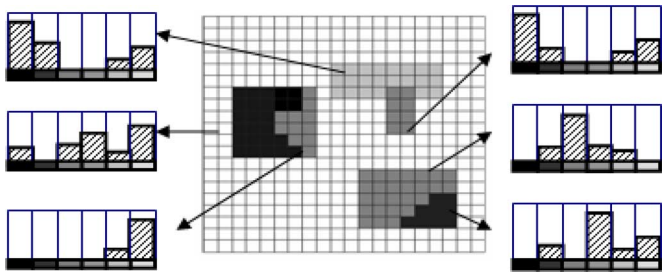

Fig. 13. Extraction of the region histogram for each of the preclassified regions.

However, in the vast majority of cases, the misclassified regions are small and in general they are connected to larger regions that were correctly classified (see Fig. 12). Based on this observation, a merging procedure for all connected regions is applied and for each region resulting from this process statistics are calculated to solve the misclassifications. Using this approach, the whole connected regions are statistically compared against the class models to decide if a particular region should be reclassified or whether two or more regions should be merged. To achieve this, the fuzzy histogram is calculated for the entire region resulting from the merging process as explained in Section II-D. The histogram merging process is illustrated in (14)

$$\mathbf{H}(\Omega) = \sum_{\forall(i,j)\in\Omega} \mathbf{Q}(i,j), \Omega = \bigcup_{i\in[1,n]} R_i \tag{14}$$

where Ω is the union of the connected regions R_i. By performing region merging, we increase the statistical relevance of the spectral-spatial vector since the merged region is significantly larger than the size of the neighborhood where the spectral-spatial vectors for each pixel in the image were calculated. Figs. 13 and 14 illustrate this process.

While the histograms depicted in Fig. 13 are calculated from image regions with different sizes, in order to compare them against the Gaussian models constructed for each class they are normalized by dividing each bin of the histogram with the number of elements that form the distribution.

In Fig. 14, each pair of connected regions are checked for merging. To do this, the region histogram is calculated for each region (H_a and H_b) and a joint histogram is calculated for the region obtained after the H_a and H_b regions are merged (H_{merged}).

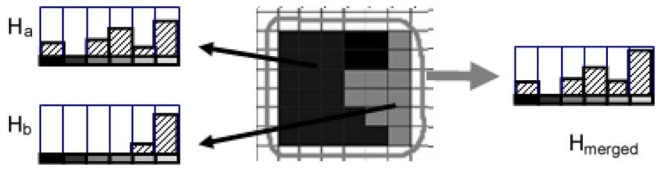

Fig. 14. Histograms of the two candidate regions (H_a, H_b) and the histogram of the merged region (H_{merged}).

The H_a, H_b and H_{merged} histograms are checked against the Gaussian models associated with all material classes stored in the database and for each histogram will be assigned a class label in agreement to the class model that minimize the matching cost.

If H_a and H_b are assigned different class labels, the probability for each region to belong to the assigned class is calculated to decide whether the regions should be merged or not. The merging probability is calculated as follows:

$$P(H_i \in C_i) = N\left(\mathbf{x}|\boldsymbol{\mu}_i, \sum_i\right). \quad (15)$$

The matching cost attained by the merged region H_{merged} (calculated using (17)) is compared against the matching costs obtained for the two separated regions H_a and H_b [see (16)]

$$P(H_a \in C_a, H_b \in C_b) = P(H_a \in C_a) \cdot \frac{N_a}{N_{merged}} + P(H_b \in C_b) \cdot \frac{N_b}{N_{merged}} \quad (16)$$

$$P(H_{merged} \in C_{merged}) = N\left(\mathbf{x}|\boldsymbol{\mu}_{C_{merged}}, \sum_{C_{merged}}\right). \quad (17)$$

To quantify the contribution of each region in (16), the matching cost for each region is weighted by the number of elements in each region (N_a and N_b) and the number of elements contained in the merged region (N_{merged}). The regions are merged if the matching cost calculated for H_{merged} is smaller than the matching cost attained for H_a and H_b.

V. Results

The validation of the proposed spectral-spatial method has been carried out in the context of nonferrous waste material classification. In this investigation the following materials are evaluated: white copper, aluminum, Stainless Steel, brass, copper, and lead (see Fig. 15).

The hyperspectral data evaluated in our study has been acquired using a PHL Fast10 CL spectral camera manufactured by Specim [11]. Although this camera is able to capture 1024 wavelengths, we elected to capture 80 uniformly distributed wavelengths in the spectral range [384.05 nm, 1008.10 nm]. The motivation behind this approach is twofold: the reduction of the onerous computational requirements to capture and process the full resolution hyperspectral data (1024 wavelengths) and to reduce the problems associated with the construction of high dimensional feature spaces (due to the high correlation between contiguous spectral bands) [46]. The illumination source consists of a mixture of halogen and near ultraviolet lamps that fully cover the analyzed spectrum range. In order to minimize the issues caused by noneven illumination, specular highlights and shadows diffuse light sources were employed.

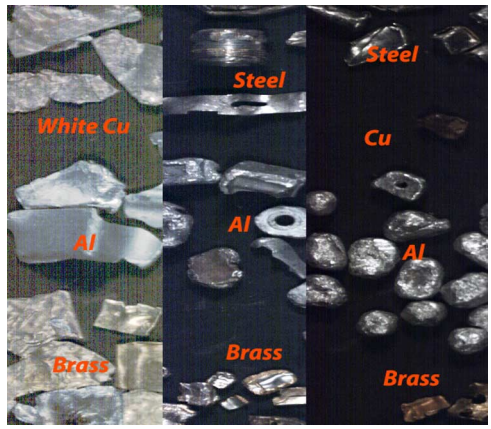

Fig. 15. The nonferrous materials investigated in this study.

The developed machine vision system consists of three independent components: the feeding device, conveyor and a part-extractor module. The shredded WEEE mixture is automatically loaded onto a nonspecular black conveyor belt (600 mm wide) via a vibratory feeder to ensure that the nonferrous materials are arranged into a thin layer prior to their arrival at the inspection line that performs the material classification in hyperspectral data. The conveyor speed was set at 20 m/min and the nonferrous materials were separated using a pneumatic part-extractor.

The material samples that were used to validate the proposed nonferrous material classification system have been provided by Indumetal Recycling S.A. and IGE Hennemann Recycling GmbH which are part of the SORMEN project consortium [2]. The nonferrous materials have been manually sorted by expert operators and in this process they use all the available knowledge about each nonferrous waste fraction. In this study, the captured datasets were divided into training and testing sets where half of the data was used for training and the remaining half was used for testing. From each of these datasets more than 500 000 spectral-spatial descriptors were extracted. The experimental results reported in this paper were only conducted on the testing datasets.

A. Background Removal

In order to remove the background information, a pixel-based evaluation proved to be sufficient to identify the background. For this operation no spectrum normalization was applied since the background does not present specular properties. The background is removed by performing a binary classification where pixel-based Gaussian models are constructed for background and nonferrous materials. The identification of the background information attained a classification rate of 97%.

B. Data Decorrelation. Classic Approaches and Fuzzy Spectral Energy Response

After removing the background information, the two different decorrelation methods discussed in Section II were tested in order to determine which method generates the best results. In

TABLE I(a)
CLASSIFICATION RESULTS USING SINGLE PIXEL SPECTRAL FEATURES

Number of features	PCA	Fuzzysets	Wavelet	RGB	LDA
2	53.08%	52.76%	51.05%		
4	61.40%	63.10%	53.96%		
8	66.43%	71.52%	63.79%	43.83%	62.86%
16	64.11%	71.43%	69.59%		
24	67.95%	71.67%	68.69%		

TABLE I(b)
CLASSIFICATION RESULTS USING SINGLE PIXEL SPECTRAL FEATURES. AUTOMATIC BAND SELECTION (FLOATING SEARCH METHOD) AND UNPROCESSED (RAW) SPECTRAL DATA

Number of spectral bands	Floating search method (FSM)	Original (raw) spectral data (80 wavelengths)
2	44.84%	
4	59.86%	
8	62.03%	
16	55.67%	
24	66.95%	
80		55.67%

this regard, one of the goals of this investigation was to calculate the optimal number of PCA components and the optimal number of fuzzy sets. The experimental results are depicted in Table I(a). In this evaluation, the classification has been carried out at pixel-level (using single-pixel spectral features). The data depicted in Table I(a) indicates that the best results are obtained when the number of fuzzy sets is selected in the range 8 to 24. Similar results were obtained when the PCA technique has been employed to decorrelate the original hyperspectral data. The experimental results shown in Table I(a) reveal that the RGB data is not sufficient to accurately capture the characteristics associated with nonferrous materials. In our experiments, when the RGB data was applied for material classification, the correct recognition rate was only 43.83%. The experimental results depicted in Table I(a) indicate that the application of the data decorrelation techniques is opportune as the classification results obtained for decorrelated data (number of features >2) are higher than the results obtained for original hyperspectral data (80 spectral wavelengths)—see the result shown in the last column of Table I(b). For comparative purposes, additional classification results obtained for other decorrelation schemes such as Wavelet decomposition [25], LDA [see Table I(a)], and automatic band selection based on floating search method (FSM) [47] [see Table I(b)] are included.

The experimental results depicted in Tables I(a) and I(b) reveal that the spectrum fuzzyfication and the classical data decorrelation methods (PCA, LDA, Wavelet and automatic band selection) produced promising results when applied to the decorrelation of hyperspectral data. However, in our experiments the proposed fuzzy sets outperformed these techniques and at the same time our approach avoids the complications associated with the training procedure required by classic data decorrelation methods that were analyzed in this study. For these reasons,

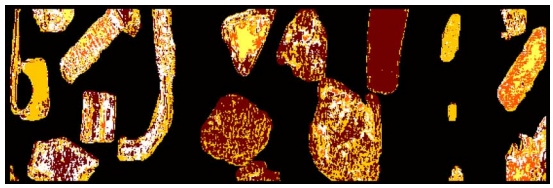

Fig. 16. Pixel-based classification results when applied to decorrelated hyperspectral data (eight fuzzy sets).

TABLE II
CLASSIFICATION RESULTS USING FUZZY HISTOGRAMS CALCULATED IN NEIGHBORHOODS OF DIFFERING SIZES

Window Size	PCA 8 features	Fuzzysets 8 features	Wavelet 8 features	FSM 8 bands	RGB
3×3	67.19%	77.30%	67.68%	71.24%	53.03%
5×5	73.77%	81.48%	72.48%	75.35%	56.14%
7×7	76.42%	83.77%	76.53%	76.84%	56.46%
11×11	78.85%	85.62%	78.34%	79.14%	57.76%
15×15	79.34%	86.45%	79.15%	80.68%	59.21%
19×19	80.41%	86.63%	80.85%	80.74%	59.83%
23×23	81.32%	86.42%	81.10%	83.78%	59.90%

the technique based on fuzzy sets was deemed as the most appropriate decorrelation method. Fig. 16 illustrates the results returned by the pixel-based classification approach when applied to hyperspectral data that was decorrelated using eight fuzzy sets.

C. Neighborhood Fuzzy Histograms

In the experiments described in the previous section, the spatial information was not included in the process of modeling the nonferrous material characteristics. In order to include the spatial information in the construction of the feature vectors, fuzzy spatial histograms are calculated for each pixel in the image data, as explained in Section II-D. To evaluate the contribution of the spatial information in the classification process, the spectral-spatial vectors (fuzzy spatial histograms) are constructed for differing window sizes. The classification process is carried out using the multivariate Gaussian classifier that has been detailed in Section III. The experimental results are depicted in Table II.

The experimental data shown in Table II indicates that the development of compound feature vectors that encompass the spectral and spatial information generates more robust image descriptors that are able to sample in a more elaborate fashion the spectral characteristics of the nonferrous materials. The results depicted in Table II prove that the decorrelation technique based on spectrum fuzzyfication produces more consistent results than PCA, Wavelet decomposition and the selection of the most discriminant bands for all window sizes and they also demonstrate that the RGB data is not suitable for nonferrous material classification. Based on the experimental data shown in Table II it can be concluded that the application of the spectral-spatial vectors for material classification proved to be opportune since the overall classification rate is increased to over 86%. An experimental example is depicted in Fig. 17.

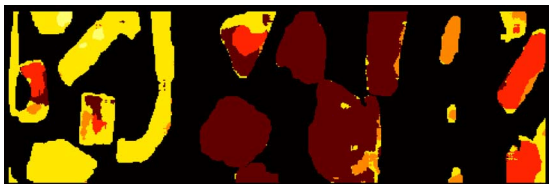

Fig. 17. Classification results using spectral-spatial feature vectors.

Fig. 18. Classification results after the image depicted in Fig. 16 has been subjected to region merging and reclassification.

TABLE III
CLASSIFICATION RESULTS AFTER REGION MERGING

Window Size	PCA 8 features	Fuzzysets 8 features	Wavelet 8 features	FSM 8 bands
3×3	75.16%	96.18%	94.18%	94.76%
5×5	93.17%	96.67%	96.13%	93.51%
7×7	94.44%	98.36%	96.02%	93.81%
11×11	92.84%	98.36%	95.65%	91.34%
15×15	92.59%	98.36%	95.75%	90.86%
19×19	92.89%	96.94%	94.75%	90.93%
23×23	92.51%	96.94%	94.68%	90.41%

TABLE IV
CONFUSION MATRIX CALCULATED FOR ALL NONFERROUS MATERIAL CLASSES (PROPOSED REGION-BASED CLASSIFICATION APPROACH)

Real / Classified	AL	Copper	Brass	Lead	Steel	White Copper
AL	97.58	0.00	0.00	0.00	0.00	0.00
Copper	0.00	98.39	0.00	0.00	0.00	0.00
Brass	0.00	0.00	96.90	0.00	0.00	0.00
Lead	0.02	0.00	0.00	98.89	0.00	0.00
Steel	2.39	1.61%	3.10	1.11	98.41	0.00
White Copper	0.00	0.00	0.00	0.00	1.59	100.00
Overall				98.36%		

Overall 98.36%.

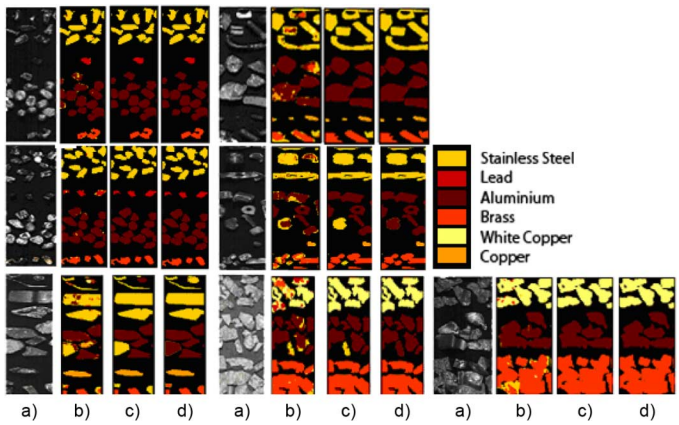

Fig. 19. Additional classification results. (a) Original image. (b) Fuzzy histogram-based classification results. (c) Results after region merging and reclassification. (d) Ground-truth image.

TABLE V
COMPARATIVE RESULTS: SINGLE-PIXEL DESCRIPTORS, FUZZY HISTOGRAMS, AND REGION MERGING

Algorithm	PCA 8 features	Fuzzysets 8 features	Wavelet 8 features	FSM 8 bands
Single pixel	66.43%	71.52%	63.79%	62.03%
Fuzzy histograms	78.85%	85.62%	76.53%	79.14%
Region merging	94.44%	98.36%	96.02%	93.81%

D. Region Merging

The regions identified after the application of the neighborhood (spectral-spatial) histograms (see Section V-C) are subjected to reclassification using the procedure discussed in Section IV. In this process for each connected region the merging cost is evaluated using the (15) and (16) and the merging decisions are based on the minimization of the matching cost criterion. The experimental results shown in Table III indicate that optimal results are obtained when the spectral-spatial histograms are calculated in a 7×7 neighborhood.

The results depicted in Table III show that the application of the region merging process reduced to a great extent the level of misclassified regions.

The confusion matrix (Table IV) constructed for all materials evaluated in this study reveals that most errors are caused by the misclassification of the Stainless Steel and the class overlap generated by nonferrous materials with similar spectral properties. Additional experimental results are depicted in Figs. 18 and 19.

To illustrate the appropriateness of the proposed spectral-spatial features, in Table V results that illustrate the improvement in performance when the classification is performed using single-pixel spectral descriptors, fuzzy histograms and after region merging are depicted. (To limit the size of the table only the results obtained when the fuzzy histograms are calculated in a 7×7 neighborhood are reported).

VI. CONCLUSION

The aim of this paper was to detail the theoretical and practical issues associated with the implementation of an integrated system for nonferrous material sorting. In our approach, the developed FUSSER algorithm addressed issues related to the decorrelation of hyperspectral data using an approach that emulates the human visual system and the development of fuzzy histograms that integrate the spectral and spatial features in a compact descriptor that is able to accurately sample the properties of the nonferrous materials. The proposed approach avoids

the requirement of complex and subjective training procedures and at the same time allows the construction of elaborate statistical models that can be applied for robust nonferrous material classification. To further improve the classification results, we have devised a region merging postprocessing scheme that is applied to reclassify the connected regions in agreement with the minimization of a matching cost criterion.

In this study, a large number of experiments have been conducted to evaluate the efficiency of the proposed system. In this regard, the experimental data reported in this paper indicates that the unprocessed (raw) hyperspectral information is not suitable to accurately capture the characteristics of the nonferrous materials. Our experiments revealed that significant improvements are obtained when the material classification is performed on decorrelated hyperspectral data. Another key issue related to the implementation of the material-sorting algorithm described in this paper resides in the integration of the spatial and spectral features in a compact image descriptor. The experimental data clearly demonstrate that considerably improved results are obtained when the characteristics of the analyzed nonferrous materials are modeled using the proposed fuzzy spectral histograms to achieve spatial feature integration. The nonferrous material classification (FUSSER) algorithm attained over 98% correct classification when applied to the identification of the WEEE scraps containing six different nonferrous materials (white copper, aluminum, Stainless Steel, brass, copper and lead).

The experimental results indicate that most errors are caused by the misclassification of the Stainless Steel. To reduce the rate of misclassification associated with this material, future work will be concentrated on the development of multiresolution classification schemes that will be applied to increase the discriminative power of the proposed spectral-spatial features. Additional future work will also explore the feasibility of implementing the proposed classification algorithm on a hardware platform in order to achieve the computational speed required for real-time operation and to investigate the application of multiple narrowband illumination arrangements to improve the discrimination between the Stainless Steel and the other nonferrous materials with similar spectral properties.

ACKNOWLEDGMENT

We would like to thank Robotiker-Tecnalia, Specim, and SORMEN Project Consortium for providing the data and the nonferrous materials that have been used in the validation of the proposed algorithm.

REFERENCES

[1] Directive 2002/96/EC of the European Parliament and of the Council of 27 January 2003, "Waste electrical and electronic equipment (WEEE)"—Joint declaration of the European Parliament, the Council and the Commission relating to Article 9.

[2] SORMEN, "Innovative separation method for nonferrous metal waste from electric and electronic equipment (WEEE) based on multi- and hyper-spectral identification project," Sixth Framework Programme Horizontal Research Activities Involving SMES Co-Operative Research, 2006. [Online]. Available: http://www.sormen.org/

[3] A. Bereciartua and J. Echazarra, "Sistema basado en identificación multiespectral para la separación de metales no férricos en WEEE en logísitica inversa," in *Proc. 1er Congreso de Logística y Gestión de la Cadena de Suministro*, 2007, (electronic proceedings).

[4] D. B. Spencer, "The high-speed identification and sorting of nonferrous scrap," *J. Minerals, Metals and Materials Society*, vol. 57, no. 4, pp. 46–51, 2005.

[5] M. Kutila, J. Viitanen, and A. Vattulainen, "Scrap metal sorting with colour vision and inductive sensor array," in *Proc. Comput. Intell. Modelling, Control, Autom.*, Vienna, Austria, 2005, pp. 725–729.

[6] E. J. Sommer, C. E. Ross, and D. B. Spencer, "Method and apparatus for sorting materials according to relative composition," U.S. Patent 7,099,433, 2006.

[7] D. A. Wahab, A. Hussain, E. Scavino, M. Mustafa, and H. Basri, "Development of a prototype automated sorting system for plastic recycling," *Amer. J. Appl. Sci.*, vol. 3, no. 7, pp. 1924–1928, 2006.

[8] A. J. Gesing, "ELVs: How they fit in the global material recycling system and with technologies developed for production or recycling of other products and materials," in *Proc. 6th Int. Automobile Recycling Congress*, Amsterdam, The Netherlands, 2006.

[9] C. I. Chang, *Hyperspectral Imaging: Techniques for Spectral Detection and Classification*. Norwell, MA: Kluwer, 2003, 0-306-47483-5.

[10] B. Tso and R. C. Olsen, "Scene classification using combined spectral, textural and contextual information," in *Proc. SPIE, ATMHUI X*, 2004, pp. 135–146.

[11] Specim Spectral Imaging Ltd. [Online]. Available: http://www.specim.fi/

[12] Z. Pan, G. Healey, M. Prasad, and B. Tromberg, "Face recognition in hyperspectral images," *IEEE Trans. Pattern Anal. Mach. Intell.*, vol. 25, no. 12, pp. 1552–1560, 2003.

[13] D. Naso, B. Turchiano, and P. Pantaleo, "A fuzzy-logic based optical sensor for online weld defect-detection," *IEEE Trans. Ind. Inform.*, vol. 1, no. 4, pp. 259–273, 2005.

[14] , H. Grahn and P. Geladi, Eds., *Techniques and Applications of Hyperspectral Image Analysis*. New York: Wiley, 2007, 10: 0-470-01086-X.

[15] D. Slater and G. Healey, "Material classification for 3D objects in aerial hyperspectral images," in *Proc. IEEE Computer Society Conf. Comput. Vision and Pattern Recognition (CVPR'99)*, 1999, vol. 2, pp. 2262–2267.

[16] G. Healey and D. Slater, "Models and methods for automated material identification in hyperspectral imagery acquired under unknown illumination and atmospheric conditions," *IEEE Trans. Geosci. Remote Sensing*, vol. 37, no. 6, pp. 2706–2717, 1999.

[17] N. Keshava, "Distance metrics and band selection in hyperspectral processing with application to material classification and spectral libraries," *IEEE Trans. Geosci. Remote Sensing*, vol. 42, no. 7, pp. 1552–1565, 2004.

[18] C. Willis, "Hyperspectral image classification with limited training data samples using feature subspaces," in *Proc. SPIE Algorithms and Technologies for Multispectral, Hyperspectral and Ultraspectral Imagery X*, 2004, vol. 5425, no. 1, pp. 170–181.

[19] G. Acciani, G. Brunetti, and G. Fornarelli, "Application of neural networks in optical inspection and classification of solder joints in surface mount technology," *IEEE Trans. Ind. Inform.*, vol. 2, no. 3, pp. 200–209, 2006.

[20] B. K. Feather, S. A. Fulkerson, J. H. Jones, R. A. Reed, M. Simmons, D. Swann, W. E. Taylor, and L. S. Bernstein, "Compression technique for plume hyperspectral images," in *Proc. SPIE Algorithms and Technologies for Multispectral, Hyperspectral and Ultraspectral Imagery XI*, 2005, vol. 5806, no. 1, pp. 66–77.

[21] C. Y. Kuan and G. Healey, "Band selection for recognition using moment invariants," in *Proc. SPIE Algorithms and Technologies for Multispectral, Hyperspectral and Ultraspectral Imagery XI*, 2005, vol. 5806, no. 1, pp. 122–130.

[22] S. Perkins, K. Edlund, D. Esch-Mosher, D. Eads, N. Harvey, and S. Brumby, "Genie Pro: Robust image classification using shape, texture and spectral information," in *Proc. SPIE Algorithms and Technologies for Multispectral, Hyperspectral and Ultraspectral Imagery XI*, 2005, pp. 139–148.

[23] D. Manolakis and D. Marden, "Dimensionality reduction of hyperspectral imaging data using local principal component transforms," in *Proc. SPIE Algorithms and Technologies for Multispectral, Hyperspectral and Ultraspectral Imagery X*, 2004, vol. 5425, no. 1, pp. 393–401.

[24] P. Tatzer, M. Wolf, and T. Panner, "Industrial application for inline material sorting using hyperspectral imaging in the NIR range," *Real-Time Imaging*, vol. 11, no. 2, pp. 99–107, 2005, Spectral Imaging II.
[25] P. Kempeneers, S. De Backer, W. Debruyn, P. Coppin, and P. Scheunders, "Generic wavelet-based hyperspectral classification applied to vegetation stress detection," *IEEE Trans. Geosci. Remote Sensing*, vol. 43, no. 3, pp. 610–614, 2005.
[26] J. Wang and C. I. Chang, "Independent component analysis-based dimensionality reduction with applications in hyperspectral image analysis," *IEEE Trans. Geosci. Remote Sensing*, vol. 44, no. 6, pp. 1586–1600, 2006.
[27] H. Kwon, S. Z. Der, N. M. Nasrabadi, and H. Moon, "Use of hyperspectral imagery for material classification in outdoor scenes," in *Proc. SPIE Series, Algorithms, Devices, and Systems for Optical Information Processing III*, Denver, CO, 1999, vol. 3804, pp. 104–115.
[28] B. Guo, R. I. Damper, S. R. Gunn, and J. D. B. Nelson, "A fast separability based feature-selection method for high-remotely sensed image classification," *Pattern Recogn.*, vol. 41, pp. 1653–1662, 2008.
[29] J. M. Geusebroek, R. Boomgaard, A. W. M. Smeulders, and H. Geerts, "Color invariance," *IEEE Trans. Pattern Anal. Mach. Intell.*, vol. 23, no. 12, pp. 1338–1350, 2001.
[30] D. Manolakis, C. Siracusa, and G. Shaw, "Hyperspectral subpixel target detection using the linear mixing model," *IEEE Trans. Geosci. Remote Sensing*, vol. 39, no. 7, pp. 1392–1409, 2001.
[31] J. Broadwater and R. Chellappa, "Hybrid detectors for subpixel targets," *IEEE Trans. Pattern Anal. Mach. Intell.*, vol. 29, no. 11, pp. 1891–1903, 2007.
[32] G. Mercier and M. Lennon, "On the characterization of hyperspectral texture," in *Proc. IEEE Int. Geosci. Remote Sensing Symp. (IGARSS'02)*, 2002, vol. 5, pp. 2584–2586.
[33] G. Rellier, X. Descombes, J. Zerubia, and F. Falzon, "A Gauss-Markov model for hyperspectral texture analysis of urban areas," in *Proc. 16th Int. Conf. Pattern Recogn. (ICPR'02)*, 2002, vol. 1, pp. 692–695.
[34] B. Ramakrishna, J. Wang, C. Chang, A. Plaza, H. Ren, C. C. Chang, J. L. Jensen, and J. O. Jensen, "Spectral/spatial hyperspectral image compression in conjunction with virtual dimensionality," in *Proc. SPIE Algorithms and Technologies for Multispectral, Hyperspectral and Ultraspectral Imagery XI*, 2005, vol. 5806, no. 1, pp. 772–781.
[35] S. Shafer, "Using color to separate reflection components," *Color Research and Applications*, vol. 10, pp. 210–218, 1985.
[36] R. T. Tan, K. Nishino, and K. Ikeuchi, "Separating reflection components based on chromaticity and noise analysis," *IEEE Trans. Pattern Anal. Mach. Intell.*, vol. 26, no. 10, pp. 1373–1379, 2004.
[37] H. Stockman and T. Gevers, "Detection and classification of hyperspectral edges," in *Proc. 10th British Mach. Vision Conf. (BMVC)*, 1999, pp. 643–651.
[38] , A. Gorban, B. Kegl, D. Wunsch, and A. Zinovyev, Eds., *Principal Manifolds for Data Visualization and Dimension Reduction*. New York: Springer, 2007, vol. 58, LNCS, 978-3-540-73749-0.
[39] C. M. Bishop, *Pattern Recognition and Machine Learning*. New York: Springer, 2006, 10: 0-387-31073-8.
[40] H. Kwon and N. M. Nasrabadi, "Kernel matched subspace detectors for hyperspectral target detection," *IEEE Trans. Pattern Anal. Mach.*, vol. 28, no. 2, pp. 178–194, 2006.
[41] S. Abe and M. S. Lan, "A method for fuzzy rules extraction directly from numerical data and its application to pattern classification," *IEEE Trans. Fuzzy Syst.*, vol. 3, no. 1, pp. 18–28, 1995.
[42] M. R. Emami, I. B. Turksen, and A. Goldenberg, "Development of a fuzzy systematic methodology of fuzzy logic modeling," *IEEE Trans. Fuzzy Syst.*, vol. 6, no. 3, pp. 346–361, 1998.
[43] A. M. Martinez and A. C. Kak, "PCA versus LDA," *IEEE Trans. Pattern Anal. Mach. Intell.*, vol. 23, no. 2, pp. 228–233, 2001.
[44] P. Comon, "Independent component analysis: A new concept?," *Signal Processing*, vol. 36, no. 3, pp. 287–314, 1994.
[45] C. I. Chang, *Hyperspectral Data Exploitation: Theory and Applications*. New York: Wiley, 2007, p. 227.
[46] S. J. Sangwine and R. E. N. Horne, *The Colour Image Processing Handbook*. New York: Springer, 1998, 0412806207.
[47] P. Pudil, J. Novovicova, and J. Kittler, "Floating search methods in feature selection," *Pattern Recogn. Lett.*, vol. 15, no. 11, pp. 1119–1125, 1994.

Artzai Picón received the M.Eng. degree in industrial engineering, the M.Res. degree in automatics electronics and control, and the Ph.D. degrees from the University of the Basque Country, Spain, in 2002, 2005, and 2009, respectively.

During the period 2000–2002, he collaborated with the Computer Image Processing Group (GTI2), Department of Systems Engineering and Automatics. Since then, he has been working as a Researcher for the Tecnalia Research Corporation, where he has been involved in over 30 research projects. His research interests include image classification and segmentation and the application of these technologies to industrial tasks.

Dr. PicónIn received the Best M.Eng. Final Project Award from Accenture Company for the implementation of a facial recognition system in 2002 and the ONCE International Research and Development Award in New Technologies for The Blind and Visually Impaired in 2006.

Ovidiu Ghita received the BE. and M.E. degrees in electrical engineering from Transilvania University Brasov, Romania, and the Ph.D. degree from Dublin City University, Dublin, Ireland.

From 1994 to 1996, he was an Assistant Lecturer in the Department of Electrical Engineering, Transilvania University. Since then he has been a member of the Vision Systems Group, Dublin City University (DCU) and currently holds a position of DCU-Research Fellow. He has authored and coauthored over 70 peer-reviewed research papers in areas of instrumentation, range acquisition, machine vision, texture analysis, and medical imaging.

Paul F. Whelan (S'84–M'85–SM'01) received the B.Eng. (Hons) degree from National Institute of Higher Education Dublin (NIHED), Dublin, Ireland, the M.Eng. degree from the University of Limerick, Limerick, Ireland, and the Ph.D. in computer vision from the University of Wales (Cardiff University), Cardiff, U.K.

From 1985 to 1990, he was employed by Industrial and Scientific Imaging, Ltd., and later Westinghouse (WESL), where he was involved in the research and development of high-speed computer vision systems. He was appointed to the School of Electronic Engineering, Dublin City University (DCU) in 1990 and is currently a Professor of Computer Vision (Personal Chair). He founded the Vision Systems Group in 1990 and the Centre for Image Processing and Analysis in 2006 and currently serves as its Director. As well as publishing over 150 peer reviewed papers, he has coauthored two monographs and coedited three books. His research interests include image segmentation, and its associated quantitative analysis with applications in computer/machine vision and medical imaging.

Prof. Whelan is a Fellow of IET, Chartered Engineer, and a member of IAPR. He served as a member of the governing board (1998–2007) of the *International Association for Pattern Recognition* (IAPR), a member of the *International Federation of Classification Societies* (IFCS) council, and President of the *Irish Pattern Recognition and Classification Society* (IPRCS) (1998–2007). He is a HEA-PRTLI (RINCE, NBIP) funded principal investigator.

Pedro M. Iriondo received the degree in industrial engineering in 1981. He received the Ph.D. degree in industrial engineering—electronics and control engineering from the University of the Basque Country UPV-EHU, Spain, in 2001.

In 1981, he began his professional activity working in different companies. In 1986, he founded the company *Adicorp* dedicated to the research, integration, and development of industrial vision systems. Since 1989, he has been an Assistant Professor with the Department of Automatic Control and Systems Engineering, ETSI of Bilbao, University of the Basque Country UPV-EHU. Currently, he is the Assistant Director of the School of Engineering of Bilbao responsible for relations with private companies. His research interest is focused in the fields of image processing, face detection and recognition, image transmission and stochastic systems.